Airship Sizing for Flying Qualities: An Automated Methodology and Applications

Carlo E. D. Riboldi,* Luca Alessi,† and Raffaello Terenzi‡
Politecnico di Milano, 20156 Milan, Italy

https://doi.org/10.2514/1.C038971

Among the most versatile lighter-than-air platforms, unmanned airships are currently being designed mostly for either low-altitude missions for close-distance surveillance, in competition with multicopter drones, or for high-altitude missions in the stratospheric layer, thus ideally complementing the role of space satellites. Correspondingly, algorithms to automatically compute global values such as the volume and mass of an airship for a desired mission performance and for assumed technologies of the components (such as the materials employed for the envelope or solar cells) have been experimented with and are documented in the literature. Building on this base, this research proposes a method where not just the parameters most typical of preliminary design are solved, but a unified automatic approach is employed to take into account requirements on static balance as well as dynamic performance in the form of characteristic time and damping of some of the eigenmodes. In this way, the outcome of the automatic sizing procedure may account not just for the requirements of the mission profile, but also potentially for static balance and for a desired level of flying qualities.

I. Introduction

AIRSHIPS are currently drawing the attention of engineers and investors in association with types of mission, where their inherent endurance and maneuverability features make them potential competitors with respect to existing machines [1]. These are mostly low-altitude monitoring missions (e.g., targeting electric power plants, suspended cables, and pipelines), currently flown with either unmanned multicopters or high-altitude missions in the stratospheric layer, where airships can provide both imagery and signal intelligence and relay capabilities, with the chance of repositioning and payload recovery not offered by space satellites. From a historical perspective, the reappearance of airships in recent years has been enabled by the development of electric power-trains and the availability of standardized and inexpensive electronics. For rotorcraft and fixed-wing aircraft, the technological boundary represented by the low energy and power density of chemically stable and long-lasting batteries has proven to be a crucial limiting factor on the feasibility of electrically powered machines by imposing severe limitations on payload, range, and endurance in flight with respect to classic fuel-burning alternatives [2–4]. Conversely, thanks to the decoupling between lift and motion inherent to airships (and in general to lighter-than-air platforms), the latter profit from a lower share of battery mass relative to take-off mass, where batteries are basically needed only for motion (furthermore, typically with dynamic pressure values significantly lower than those for an aircraft or helicopter), trajectory steering, and attitude control. Additionally, concerning control, smaller electric motors coupled with propellers can be put on board in a distributed fashion, enabling the exploration of many different topologies to potentially tackle controllability issues from the start of the design phase [5–7]. This makes electric motors an ideal technology for overcoming the lower control performance afforded by traditional, bulkier, and heavier piston engines, typically put on board in a very limited number and in the lower part of the airship for balancing reasons. The simplification in the management of electric motors and the fusion of the control of the power-train (including the power sources), onboard sensors for navigation, and the remote transmission of signals, all allowed by the availability of inexpensive flight control computers, allow designers to study and implement partially or fully automatic flight control and navigation suites, coping with the inherent features of a novel topology without overwhelming cost or complexity [6,8,9].

Techniques for designing novel airships have received discontinuous attention in the literature over the years, with relevant modern works carried out in the 1970s [10,11], 1990s [12], and early 2000s [13–15], and more recently culminating in the Lockheed Martin and Northrop Grumman endeavors in the field of hybrid airships [16], as well as in experimental platforms for high-altitude applications, notably the Hi-Sentinel campaign [17,18]. Currently, some of the most advanced designs are led directly by companies without major disclosure to the general public [19–22], with the notable exception of the EU-funded project IPROP [23], where, within a larger scientific scope including the development of ion-plasma propulsion technology for airships, a significant effort is being devoted to experimentation with airship design methods and airship modeling.

The problem of preliminary sizing of an airship has been tackled in good detail [1,16,24], allowing one to link the specifications corresponding to a desired mission profile (e.g., payload, cruising altitude, endurance) and the assumed technology of the components (material density of the envelope or solar cells, thrust-to-weight ratio and efficiency of the electric motors and propellers, power-to-weight ratio and energy-to-weight ratio of the batteries, etc.) to a prediction of the take-off mass, its corresponding mass break-down, detailing the mass of each component, and the overall volume of the envelope. A mass-optimal approach has been attempted [25,26], including solar cells in the design of a high-altitude airship and exploiting assumptions on the relative position with respect to solar irradiance so as to size them in the most mass-efficient way (a procedure extended also to the case of an airship for Martian exploration [27]). For the purpose of solving the problem of static balance, and, in particular, the mutual positioning of the center of gravity and the center of buoyancy of the airship, tools for detailed lofting can be employed so as to envisage a suitable positioning of the components (with associated mass and external volume) on board, typically in a subsequent design phase with respect to preliminary sizing. Actually, accurate static balancing operations are not infrequently carried out only by hand once the airship has been manufactured. Flight performance and dynamic analysis based on rigid-body assumptions and mid-fidelity aerodynamics have been deployed sporadically to assess the performance of existing airships,

Received 9 February 2026; accepted for publication 28 April 2026; published online Open Access 17 June 2026.

*Associate Professor, Department of Aerospace Science and Technology, Via La Masa 34; carlo.riboldi@polimi.it (Corresponding Author).

†Research Assistant (MoS), Department of Aerospace Science and Technology, Via La Masa 34.

‡Ph.D. Candidate, Department of Aerospace Science and Technology, Via La Masa 34.

including in the presence of control, in particular investigating the effect of a different layout of the thrusters, or of a different shape of the envelope, on performance indices such as maximum climb/dive speed or damping of the eigenmodes [6,7,15,28].

Making use of pre-existing separate tools employed in the various phases of the design, as just highlighted, the present research proposes a unified design methodology that links them physically within a single numerical procedure. In particular, by exploiting the potential of each of the three tools just mentioned—for preliminary sizing, lofting/inertia modeling, and flight performance analysis—the designer is allowed to set design goals that from the start are not limited to the mission profile but include the satisfaction of static balance constraints as well as dynamic performance indices, thus in particular granting the satisfaction of a certain level of flying qualities.

Taken one by one, the tools employed for each of the design stages have been developed and implemented for previous research and are well documented in the cited literature. Therefore, after summarily outlining their features relevant for the task at hand, the focus of this contribution is shifted to the analysis of a proposed framework for setting and checking compliance with static balance and flying-quality requirements. The latter are not defined by regulations for airships with the same level of detail as for other classes of flying machines, thus requiring some elaboration. The overall loop of the design process will be described, and practical results will be shown for the case of an existing preliminary prototype of an airship developed for layout testing within project IPROP, further demonstrating the potential of the proposed methodology through parameterized design studies.

II. Modules for an Airship Sizing Methodology

In this section, the structure of three independent modules conceived, respectively, for the preliminary sizing of lumped parameters (take-off mass break-down, volume, etc.), lofting and static analysis, and dynamic simulation and eigenanalysis of airships, is summarily described. In the next section (see Sec. III), it will be shown how they can be profitably linked, so as to generate a unified design tool.

A. Preliminary Sizing Methodology

In the following, the baseline procedure for airship sizing considered in this work will be outlined at a conceptual level (Sec. II.A.1). Details on possible implementations (e.g., regression models) can be retrieved from the existing literature. Subsequently, relevant additions to the baseline procedure, adopted to make it a module of a broader sizing tool, will be presented (Sec. II.A.2).

1. *Outline of the Baseline Procedure*

Considering a non-rigid airship, the preliminary sizing phase, leading to the definition of its take-off mass, the corresponding break-down into mass values pertaining to onboard components, and the overall volume of the airship envelope, can be formulated analytically in its simplest form as a single non-linear algebraic equation in one unknown. The latter is representative of the geometrical sizing and can be assumed to be the length L of the airship envelope. The geometry of the envelope can be assigned by means of a single design parameter, provided that a suitable shape function has been defined to assign a complete shape geometry as a function of a single parameter only. Suitable shapes already employed in the literature are, e.g., bi-ellipsoidal, like the low-drag example developed by NPL, consisting of two halved bi-axial ellipsoids joined at the cross section of maximum thickness; cylindrical with semi-ellipsoidal caps; or polynomial, where an axis-symmetric envelope shape is obtained through revolution around the longitudinal axis of a segment of a high-order polynomial defined in the plane of symmetry of the airship [16,25,28]. The key point in all of these examples is that, by pre-assigning proportions (e.g., the ratio of semi-axes for ellipsoids), a sized geometry is obtained simply by specifying the parameter L.

In order to find the value of the latter in an automatic way, the following procedure, called iteratively, can be employed (see Fig. 1). First, a design parameter typically defined by the designer, and considered known within the sizing procedure, is the buoyancy ratio BR, defined as the ratio of buoyancy to weight. The latter is typically over 90% in most existing designs, closer to 100% for airships mostly designed for hovering and less for those designed for advancing flight. In the latter case, the additional dynamic lift exerted by the envelope and horizontal tail, given by trimming the airship with a non-null angle of attack, fills the gap between weight and buoyancy. For so-called dynamic airships instead, BR may drop to much lower values, and the dynamic lift from the envelope would become more substantial (increasing the relevance of a high lift-to-drag ratio provided by the selected envelope shape, which is otherwise far less relevant than it is on winged aircraft, in particular). Then, environmental and technological parameters for the sizing need to be assigned and considered constant in the sizing process. Starting from the assignment of these constant quantities and from a target BR, for a given value of the envelope length L, assumed known within an iteration of the solver, it is possible to invoke a set of models and regressions, producing the mass sizing of all major subsystems on board. This set of instructions—namely, the *sizing loop*—constitutes a procedure that is called repeatedly within the solver, updating the value of L in search of a sizing solution. The operations within the sizing loop can be synthetically described as follows (Fig. 1) and are quantitatively detailed in [16,24,25].

1) *Geometrical Sizing of Envelope*. Through the assignment of the free geometrical parameter L, it is immediately possible to compute a sized geometry of the airship envelope, thus defining in particular its volume Vol, area of the external surface, and top areas of the cross and longitudinal sections. An estimation of the zero-lift drag coefficient can be carried out based on regressions for the envelope. Similarly, refinements of this preliminary estimation of drag can be carried out based on the geometrical size of the fins and gondola (if any), themselves obtained from regressions of statistical data given the size of the envelope.

2) *Environmental Conditions Along the Mission Profile*. The mission specifications need to be assigned in terms of velocity and time duration (or range) of each leg, typically including (at least) climb, cruise, and descent. With knowledge of the duration of

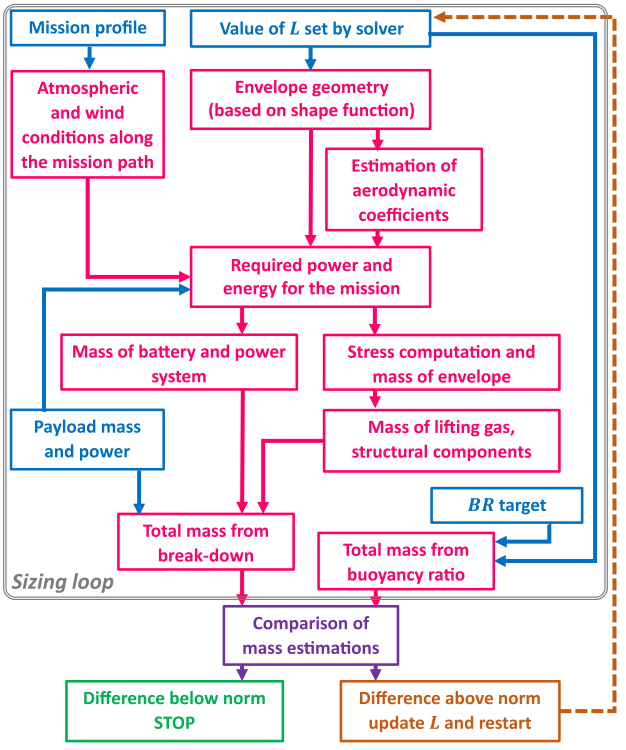

Fig. 1 Conceptual workflow of the baseline airship sizing methodology.

each leg, it is possible to find nodal values of position and altitude over a discrete grid of time instants. Through the assignment of the position on Earth and the time of year for the start of the mission, for each of these nodal altitude conditions, it is possible to compute, from dedicated models, the temperature, pressure, and density of air and the wind intensity and direction. In particular, the International Standard Atmosphere (ISA) model can be employed for static air characteristics and the Horizontal Wind Model (HWM) for the wind characteristics [29,30].

3) *Computation of Total Power and Energy Required*. Having obtained knowledge of the wind characteristics along the climb and at altitude, as well as the ground speed as part of the mission profile, it is possible to define the airspeed and the corresponding peak power and energy required for a mission profile. For simplicity, it is assumed that the airship is flying in a climb at a negligible angle of attack and with a given climb angle and is always oriented with the plane of symmetry normal to the plane of the horizon and aligned with the wind so that no side-slip occurs. This allows one to preliminarily estimate the drag coefficient through the reference value for a null angle of attack and side-slip. In the cruise legs at constant altitude, the value of the drag coefficient is increased by a safety factor with respect to the purely reference value on account of the side-slip angle resulting from a misalignment between the airship heading and track, resulting from the potential difference between the directions of the ground and wind velocity vectors. The estimation of power for propulsion is therefore possible with these elements, in the same fashion as for winged aircraft. Power for propulsion is complemented by the power required for the payload, as well as that required for the other plants on board, including losses (estimated via regressions or directly assigned, corresponding to the specific technology of each powered component). Once the power along the mission profile is known, the peak power and the energy required for the mission are easily obtained.

4) *Computation of Available Power and Energy.* By comparing the peak power required and the energy required for the mission, the candidate sizing of the battery is obtained, employing both quantities in parallel, and the values of the energy-to-mass and power-to-mass ratios typical of the selected battery chemistry, as well as a corresponding charge/discharge efficiency.

5) *Mass of Power System*. The power required for flight allows one to define the power of the motors, propellers, and their nacelles/mountings. Given an assigned number of motors N_m, this yields the overall mass of these components, lumped in M_m for the motors and propellers, and M_{mm} for the mountings. These masses are complemented by those of the power-trains and sub-plants (cables, power electronics, etc.), through technological regressions, yielding the component M_{mc} for the motor control components. Finally, the mass of the power system includes that of the battery M_b, obtained starting from its respective sizing (see previous point). In particular, the mass of the battery is chosen as the more stringent of the two candidates.

6) *Stress Analysis on Envelope*. With knowledge of the dynamic pressure along the mission and of the maximum wind speed to sustain (specified among the assigned technological parameters), as well as of the external pressure, it is possible to compute the pressure differential, the hoop stress, and the longitudinal stress on the envelope from regressive models. The rationale behind these models is that a minimum pressure differential across the envelope needs to be achieved, primarily to avoid caving of the envelope and to ensure sufficient stiffness of this aerodynamic-load-bearing component. Statistically, the tension differential corresponds to values of the planar stress that the envelope needs to sustain.

7) *Mass of Envelope and Structural Components*. The area density of the envelope material can be obtained as a material-specific (typically) linear function of the maximum stress to be sustained, computed at the previous point. For safety, a multiplication factor of 4.0 is applied to the maximum stress, in accordance with existing civilian regulations and on account of the coarse nature of the structural model. With knowledge of the geometrical sizing of the envelope (from the initial point) and of the areal density, its mass M_{env} can be readily computed. Clearly, a larger value of the areal density is representative of more plies in a multi-layer material, or of a greater thickness for homogeneous single-layer envelopes. The mass M_{lg} of the lifting gas and the related mass M_{ps} of the pressure system required to fill and pressurize the envelope are computed at this step as well, together with the masses of structural parts such as the fin empennages M_t and inner diaphragms M_{dia}, which are functions of the size of the tail, in turn obtained from that of the envelope at point 1), and of the airspeed.

8) *Mass from Break-down and from Buoyancy Ratio*. The mass of the gondola M_{gon} can be estimated via regressions from the known mass of the payload M_{pl}. Finally, the mass of the entire airship can be obtained from the corresponding break-down, where the mass of each component has been estimated from previous points, as in Eq. (1),

$$M_{\text{break-down}} = (M_{env} + M_{dia} + M_{lg}) + M_t + (M_m + M_{mm} + M_{mc}) + (M_b + M_{ps} + M_{gon} + M_{pl}) \tag{1}$$

In parallel, another estimation of the airship mass can be obtained from the buoyancy ratio BR, the volume of the airship Vol and the density of the air ρ_{air} at a reference altitude, as in Eq. (2),

$$M_{\text{buoyancy}} = \frac{\rho_{\text{air}} \cdot \text{Vol}}{\text{BR}} \tag{2}$$

A numerical solver for non-linear equations attempts to balance M_{buoyancy} and $M_{\text{break-down}}$, obtained via independent estimations at the last point of the procedure, by iteratively changing the envelope length L, thus analytically yielding the non-linear Eq. (3),

$$M_{\text{buoyancy}} = M_{\text{break-down}} \tag{3}$$

The method just outlined can be extended or modified depending on the application, including more sophisticated models for the existing components (such as first-principle models instead of regressions for linking technological and geometrical specifications to the mass estimation for a component) or including more components. Notably, developments including solar cells have been presented in the literature, giving rise to a problem more suited to an optimal solution and requiring sophisticated modeling of the solar irradiance (in terms of intensity and direction) at nodal points along the mission [25]. In that case, the number of unknowns in the sizing problem is extended, encompassing those needed for the geometrical sizing of the solar cells. Furthermore, the exposure of the panels to different irradiance depending on the geographical coordinates and time of day and year is taken into account for correctly assessing the contribution to the power balance. The sizing problem is configured as a mass-optimum-seeking optimization. In another analysis, a similar approach to the latter (i.e., optimum-seeking) has been considered, further including the sizing of ion-plasma thrusters, which induces more geometrical sizing parameters related to the front area of the thrusters in the sizing problem [24].

However, the key common point in the baseline technique just outlined here, on the one hand, and the variations just mentioned and documented in the literature, on the other, is that the output of this preliminary sizing procedure is invariably made up of at least the total mass M_{TO} and its break-down as in Eq. (1) (with additional components, such as those for solar cells, on the right-hand side of the equation, where needed in the design), as well as the geometrical definition, in terms of shape and sizing, of the envelope and, notably, the sizing in terms of area S_{ht} and S_{vt} of the horizontal and vertical tail empennages, as well as their longitudinal positioning from the center of buoyancy CB, all obtained as side products of the estimation procedure for the tail mass M_t. Such estimation is carried out according to a statistical approach, based on the current values of the length L and volume Vol of the envelope.

2. *Modifications to the Baseline Procedure*

Conversely, the features of the design solution that are not computed or specified at this level include the position of the center

of buoyancy of the airship CB, the center of gravity CG, and the geometrical sizing or positioning of the components on board. This indetermination, while typical of preliminary sizing, needs to be tackled in the present work, in view of the employment of the sizing procedure outlined above as a module within a broader design method in which lofting is included. Correspondingly, an amendment to the baseline procedure is introduced here, specifically targeting the static balance of the airship at a preliminary sizing level.

Assuming a body reference $\mathcal{B}$ centered in CB, as is typical in the field of airship dynamics modeling [6,14,15], such that the vertical plane of symmetry is normal to the rightward-pointing unit vector $\boldsymbol{b}_2$, consider that $\boldsymbol{b}_1$ is pointing forward and $\boldsymbol{b}_3$ toward the bottom of the airship (in a similar way as traditionally for winged aircraft), as in Fig. 2. The coordinates of a point with respect to the body reference $\mathcal{B}$ (with unit vectors $\boldsymbol{b}_1$, $\boldsymbol{b}_2$, $\boldsymbol{b}_3$) can be defined as (x, y, z). For symmetry it makes sense to exclude any sideward displacement of CG and CB; hence, $y_{\mathrm{CB}} = y_{\mathrm{CG}} = 0$. Furthermore, within the plane of symmetry of the airship, the position of the CG needs to be nearly or exactly below that of CB, or

$$x_{\mathrm{CG}} = x_{\mathrm{CB}} + \Delta_{\mathrm{CG,trim}} \tag{4}$$

In Eq. (4), $\Delta_{\mathrm{CG,trim}}$ represents a nominal longitudinal misalignment between the CG and CB, specified by the designer such that it recovers, through the moment of gravity with respect to the reference point CB, the aerodynamic moment induced by the envelope and tails in a nominal trimmed condition (typically in cruise). When $\Delta_{\mathrm{CG,trim}} = 0$, as is typical of slowly advancing or mostly hovering airships, the two centers are longitudinally aligned $x_{\mathrm{CG}} = x_{\mathrm{CB}}$. Additionally, concerning the vertical placement, for static balance it is required that $z_{\mathrm{CG}} > z_{\mathrm{CB}} = 0$, implying that the center of gravity lies below the center of buoyancy.

Now, in particular, the requirement on longitudinal misalignment in Eq. (4) can be easily turned into an additional equation in the solver for initial sizing. Since this is a single scalar equation, only one additional unknown can be included in the problem. This has been identified as the longitudinal positioning of a set of items, among those associated with mass in Eq. (1), considered movable within the general layout of the airship. In particular, it is reasonable to assume that the gondola and everything in it, namely, the batteries, payload (which may include a flight control system), and pressure system, can be displaced longitudinally by a quantity $\bar{x}$ with respect to the CB, so as to satisfy Eq. (4). Then, an additional computational procedure within the sizing loop of the iterative solver introduced in Sec. II.A.1 has been defined, considering now the two independent variables $\bar{x}$ and L assigned and known at a given iteration. Following from point 8) above:

9) *Position of the Center of Buoyancy.* The position of the center of buoyancy CB of the airship can be estimated at this stage based on the prevailing contribution of the envelope only and correspondingly computed for a given geometry of the envelope.

10) *Positioning of the Non-movable Components*. The non-movable components can be categorized into two groups, respectively, either positioned in relation to CB or assigned by the designer. Referring to the elements mentioned in Eq. (1), in the first group are the envelope, lifting gas, longitudinal diaphragm, and tail empennages. The center of gravity of each of the former three can be estimated at the center of buoyancy, at least for a non-rigid airship. The latter, as pointed out, are sized at this level in a statistical way, and their positioning x_t with respect to the CB comes as a side product of their mass sizing within the baseline procedure [16,25,26]. In the second group are the motors, their mountings, and powering/control wiring, positioned such that their relative center of gravity is located at x_m, assigned by the designer.

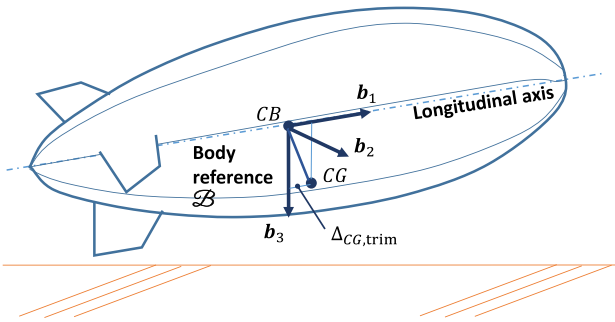

Fig. 2 Body reference, positions of centers CB and CG. Definition of $\Delta_{\mathrm{CG,trim}}$.

11) *Estimate the Position of the Center of Gravity.* The position of the center of gravity CG (from CB, which is the origin of the reference, as stated) can be computed according to the following Eq. (5):

$$x_{\mathrm{CG}} = \frac{(M_b + M_{ps} + M_{gon} + M_{pl})\bar{x} + M_t x_t + (M_m + M_{mm} + M_{mc})x_m}{M_{\text{break-down}}} \tag{5}$$

The numerical solver will call the so-defined procedure iteratively, updating $\bar{x}$ and L and simultaneously trying to balance $M_{\text{break-down}}$ with M_{buoyancy} [Eq. (3)], and x_{CG} with x_{CB} according to Eq. (4).

Within the present research, the procedure just outlined has been implemented in a suitably modified version of the software `Morning Star`, an in-house-developed suite working in Matlab®, allowing for the initial sizing of an airship. Conceived as a stand-alone code, it is employed here as a module within the global design methodology described later in this paper (Sec. III).

B. Lofting for Detailed Static Analysis

A crucial passage when moving from the topological model obtained as an output of the preliminary sizing phase (Sec. II.A) toward an item that is physically manufactured, lofting corresponds to producing a detailed geometry and mass distribution. In this process, the adopted modeling strategy makes use of an assembly of bodies, each represented either as one or more discrete masses (or point masses) or as a solid with distributed mass. The criteria for selecting the actual type of mass representation may vary; yet the target output of this type of modeling is an accurate computation of the center of mass and external volume (hence buoyancy), as well as characteristics stemming from the distribution of mass and volume, namely, the center of mass and center of buoyancy. Additionally, the static moment and moment of inertia can be computed from the mass distribution as well, which are typical inputs for a dynamic analysis [6,7].

The additional input required to set up a detailed three-dimensional representation with respect to a topological model is essentially some knowledge of the geometry and physical construction of the components (in particular, whether the density of an item modeled as a finite body can be considered constant). This unavoidably makes this modeling stage specific to a given design, since the geometry and construction of the same item (e.g., the gondola) may change depending on the specific design problem.

In this research, taking inspiration from the experience gained in the design and manufacture of the airship prototypes within project IPROP [9], we consider the components of the major elements composing the topology of the airship, corresponding to components in the airship mass break-down (Sec. II.A.1), specifying what type of modeling has been adopted for each of them.

1) *Gondola*. The mass of the gondola M_{gon} conveys that of the actual body (holding the payload, batteries, and pressure system), and that of the anchoring system employed for linking the gondola to the envelope. Additionally, if the motors are attached to the gondola in the design at hand, the struts to which the motors are physically attached, stemming from the gondola, are considered part of the weight of the gondola as well. Since the gondola and struts are associated with a significant mass and physical extension, and their shape is assumed known, they are modeled here as finite bodies, and the construction features are modeled correspondingly. Conversely, the anchoring devices, typically patches applied to the envelope and cables connecting the gondola to the envelope, are considered

lumped masses, located at the position of each anchoring point. The payload, batteries, and pressure system, associated with a corresponding mass each (M_{pl}, M_b, M_{ps}), are modeled as point masses, located at the center of gravity of the gondola structure, on account of their limited geometrical extension.

2) *Empennages*. The mass of the tails M_t conveys also that of the corresponding anchoring points and of the actuators (if present). A relevant stage in the lofting process of the airship is that of assuming a tail configuration. Whereas at a preliminary sizing stage the sizing of the tail defines the horizontal and vertical areas (S_{ht}, S_{vt}), in the lofting phase a tail assembly such that it produces those areas should be defined. The most straightforward choice is that of a cruciform tail with distinct vertical and horizontal empennages. In that case, the area of the horizontal and vertical empennages can be translated into correspondingly oriented empennages. However, even in that layout, the vertical empennages at the top and bottom of the envelope may be differently sized, still complying with the global S_{vt} area constraint, but producing a markedly different geometry. Then, clearly, noncruciform tails can be considered, such as Y or inverted-Y configurations, X-configurations with diverse values of empennage dihedral, etc. The empennages are typically among the most geometrically sizable items on board; hence, following a selection of their arrangement, their assumed geometry is employed for carrying out a finite-body representation of the corresponding mass distribution, although typically considering a simplified homogeneous solid with an isotropic density such that it complies with the available mass, irrespective of the actual structural construction of these surfaces, for which often insufficient information exists at this stage. The anchoring patches and the actuators can be treated conversely as point masses.

3) *Envelope and Lifting Gas*. The geometry of the envelope is already known from the preliminary sizing phase (see Sec. II.A.1). The envelope mass M_{env} conveys also that of jointing strips, which are employed for soldering the envelope segments to one another. Considering a non-rigid construction, the envelope corresponds typically to the gas-tight component of the machine. The envelope is modeled as a hollow body with a given thickness, whereas the cavity within the envelope can be modeled as a finite body with the density property of the lifting gas, and holding its mass M_{lg}. The envelope strips can be modeled as finite bodies, provided that their geometry is known, or alternatively as sets of point masses along the chin line where they are laid. If present, a diaphragm, typically put on board for structural reasons to help keep the shape of the envelope (and associated with M_{dia}), can be modeled as a finite body.

4) *Motors*. Motors, mountings, and motor control systems, associated with M_m, M_{mm}, and M_{mc}, respectively, are split by the number of motors on board, N_m. The latter needs to be defined at this level, whereas it is not strictly needed for the power balance computation carried out in the preliminary sizing phase. The mass of the motors conveys those of the electric motors and propellers, assuming a standard electromechanical thruster. These items are typically very compact compared to the overall topology of the airship and are treated here as point masses.

It should be remarked that the modeling approach introduced in the listing just given is not general. For example, if the gondola is very compact, or its actual shape or construction strategy is not yet finalized, it makes sense to model it as a point mass, located at the position of its center of gravity. Clearly, the results in the computation of the center of buoyancy and moment of inertia will be correspondingly affected.

Another remark concerns the link between the preliminary sizing phase (see Sec. II.A) and the lofting phase considered here. The simplified models invoked throughout the preliminary sizing phase for linking a set of design variables to the mass of a component typically assume the use of a material and of a manufacturing technology. For example, the prediction of the tail mass will be different depending on whether the empennages are made of filled polystyrene or of a hollow aeronautical beam in wood or metal. When linking a preliminary design module to a lofting module in a design procedure, the choice of the materials and construction of the components is very relevant, since the construction is reflected in the lofting of the actual geometry when employing a finite body for the modeling. For example, whether the tail is filled or hollow may correspondingly change the assignment of the properties of the empennages in the model for the lofting phase.

When completed, the model with geometry and masses enables the computation of the center of buoyancy and center of gravity in a more accurate way with respect to the preliminary sizing. The center of buoyancy is influenced by the actual volume of the material; hence, in particular, the tails, especially when filled (as is typical of smaller airships where they are made of polystyrene or a similar material), contribute through a residual percentage of the overall buoyancy but more significantly to the positioning of the center of buoyancy CB, since they are concentrated at the back of the airship. Similarly, the actual geometry of the tail, not accounted for in the preliminary sizing phase, may produce alterations to the center of gravity after the lofting phase, e.g., on account of the geometrical constraints originating from the actual mating of the tail shape with that of the envelope. In Sec. III, a proposed way to deal with these mismatches will be introduced.

In this research, the lofting phase has been carried out employing an in-house-developed library called `AFL`, a shortcut for `Assembly Features Library`. Designed as a multipurpose, easily linkable, object-oriented library in Matlab®, as shown in an example in Fig. 3, `AFL` in this context allows the designer to specify an airship topology, completed by mass-density properties for finite

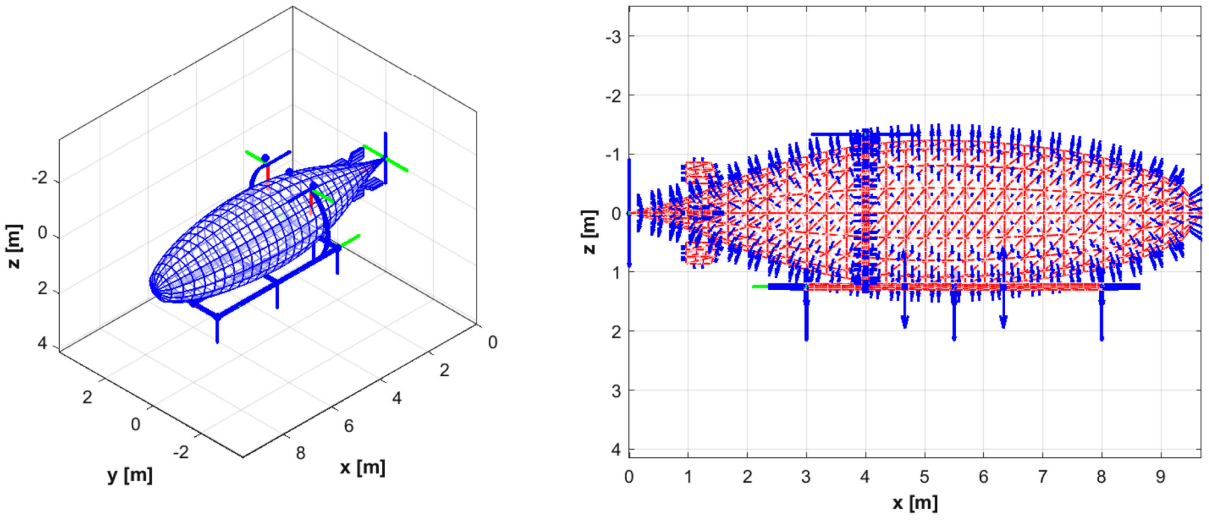

Fig. 3 Example lofted model of an airship in `AFL`. Left: topology model with point masses and finite bodies. Right: discrete representation of the finite bodies.

bodies and by masses for lumped-mass components. It carries out the computation of buoyancy and inertia properties (including the position of the center of gravity CG and of buoyancy CB, as well as the overall buoyant volume, mass, and inertia tensor components with respect to an arbitrary point or reference) required for assigning a dynamic model, offering also the option to efficiently update these properties where needed, e.g., when changing the configuration of an assembly during a time-marching dynamic simulation.

C. Dynamic Modeling

The last module needed within an airship design technique such that it accounts for flying qualities is a dynamic model of the airship. A mid-fidelity model for the dynamic analysis of the airship has been proposed and employed by the authors, and it is detailed both in terms of formulation and potential applications elsewhere [6,7]. However, for easier readability of this paper, the major features of the adopted modeling will be summarized here. They are physically implemented in the in-house-developed library SILCROAD, a shortcut for Simulation Library for Craft-Object Advanced Dynamics, which is a multipurpose, object-oriented library programmed in Matlab®, conceived for the easy simultaneous simulation of multiple flying bodies (possibly of different classes, such as fixed-wing aircraft, airships, missiles, etc.). The adopted approach includes provision for an arbitrary definition of the reference point for writing the non-linear equations of motion of a flying craft; an accurate definition of the positions of the centers CG and CB, of the volume, mass, and inertia tensor (fully populated); and for the accurate positioning on board of an unlimited number of fins and thrusters (with arbitrary orientations). For thrusters, a thrust model allows one to modulate the intensity of each thrust vector with respect to a throttle control variable, as well as a function of velocity (or Mach number) and altitude. For fins, each comes with a deflectable trailing-edge surface, which allows for corresponding aerodynamic control.

For an airship-class object, SILCROAD allows one either to specify stability and control derivatives, or, conversely, to provide the input required to set up an aerodynamic model as described by Munk–Jones–DeLaurier theory [11,31] for the envelope part. In essence, the actual shape of the envelope can be specified by the user, and a discrete representation of the airship volume along the longitudinal axis is carried out. For each discrete element, a method for computing three local components of aerodynamic force and the corresponding contributions to moment is implemented [11]. For this computation, the method accounts for the local value of the airspeed vector itself due to the linear velocity and rotational rate of the body and to the local acceleration vector [32]. The aerodynamic model estimates the drag according to an attached-flow and a crossflow effect, thus allowing it to effectively capture the behavior of the airship also for rather high angles of attack [33], which might be encountered on an airship more easily than on a winged aircraft [14], for instance, when maneuvering in near-hover conditions [7]. The contribution of the envelope to the overall aerodynamic actions on the airship is extended from the nose to a longitudinal station defined by the user in proximity to the leading edge of the root airfoil of the tails. Provision is made for specifying three-axis components of apparent inertia of the envelope [31,32].

The fins are treated according to a lumped model, where lift, drag, and moment coefficient sensitivities specified as parameters are employed to compute aerodynamic forces and torque due to attached flow and crossflow components [34], and knowledge of the positions of the aerodynamic center and crossflow force center allows one to compute the overall moment due to the aerodynamic forces.

The non-linear model can be employed to derive a corresponding linearized model, which, for a given reference condition (typically, a static trimmed flight), is obtained by writing the inertia components explicitly and by computing active force and moment sensitivities through a perturbation approach, where aerodynamic, propulsion, gravity, and buoyancy forces and moments are considered one by one, and their change with respect to the value in the reference condition is computed when perturbing the airship states (specifically, the body components of velocity and rotational rate and the three attitude angles in a Tait–Bryan sequence [35]) and controls (deflectable aerodynamic surface controls around the three body axes and the settings of each of the thrust levers) in the model one by one. The availability of a linearized model enables linear analysis, in particular the efficient computation of eigenvalues and eigenvectors [28]. The ease of synthesis of a linearized model is an asset for performing parameterized analyses by computing the model for different reference conditions, typically differing in terms of reference airspeed.

III. Unified Design Methodology: From Preliminary Sizing to Dynamic Characterization

As stated in the Introduction (Sec. I), the three modules listed in the previous section, originally conceived each as a stand-alone tool, can be linked to one another, thus allowing the designer to include from the start a set of requirements on static and dynamic performance. The overall process with the additional design targets enabled by the procedure just explained is schematically shown in Fig. 4.

A. Conceptual Aspects in the Intermodular Links

Two major conceptual aspects require comment. First, as pointed out in Sec. II.B, the results of the preliminary sizing module are not generally consistent with those of the lofting module from the start. This is due to the more detailed definition of the geometry of finite bodies in the lofting module and the corresponding more precise computation of the positions of the centers CG and CB. To increase consistency, in the proposed unified workflow, the first two modules are joined within the iterative loop leading to the preliminary sizing solution. In particular, the lofting phase is positioned between points 8 and 9 within the procedure described in Sec. II.A. This clearly means that additional assumptions on the geometry and construction of the components with respect to those required for preliminary sizing need to be made before running this first unified loop. In particular, the following aspects need specification:

1) The detailed geometry and material of the gondola structure, which is modeled with finite body elements, and the number and mass of the anchoring structures of the gondola to the envelope.

2) The configuration and detailed geometry of the empennages in the tail, modeled as finite body elements, and the position and mass of the anchoring devices and actuators for each of them.

3) The number of thruster units and their positioning with respect to the envelope (the latter allows one to define the detailed sizing of the struts protruding from the gondola, which are modeled as finite body elements).

4) The position of diaphragm(s) within the envelope.

It should be observed that making these assumptions requires some additional data to be known before launching the design computations. Correspondingly, these data shall be employed for selecting more accurate regressive or first-principle models within the preliminary sizing module, thus ensuring better consistency between the first two modules. This applies in particular to the gondola, the empennages, and the anchor points. To explain this, consider as an example the construction and material of the gondola, and assume that it is known to be made of a number of sticks of balsa wood glued together, forming a frame with a prescribed shape (for instance, rectangular with diagonals). The geometrical sizing of the gondola can be bound to that of the envelope (e.g., its length and width can be proportional to the length L and radius of the envelope), but for a given geometrical size, the mass can be computed with absolute precision by knowing the density features of the material and the cross section of the sticks at the level of preliminary sizing. Lofting will need the geometrical sizing for inertia and buoyancy computation, requiring also the radial positioning of the gondola with respect to the envelope. In a similar fashion, it is possible to treat the tail empennages.

By adopting this link between the preliminary sizing and lofting modules, it is possible to profit from the accurate knowledge of the centers CB and CG as obtained from the lofted model (in this implementation, within AFL) to compose Eq. (4) within the solving

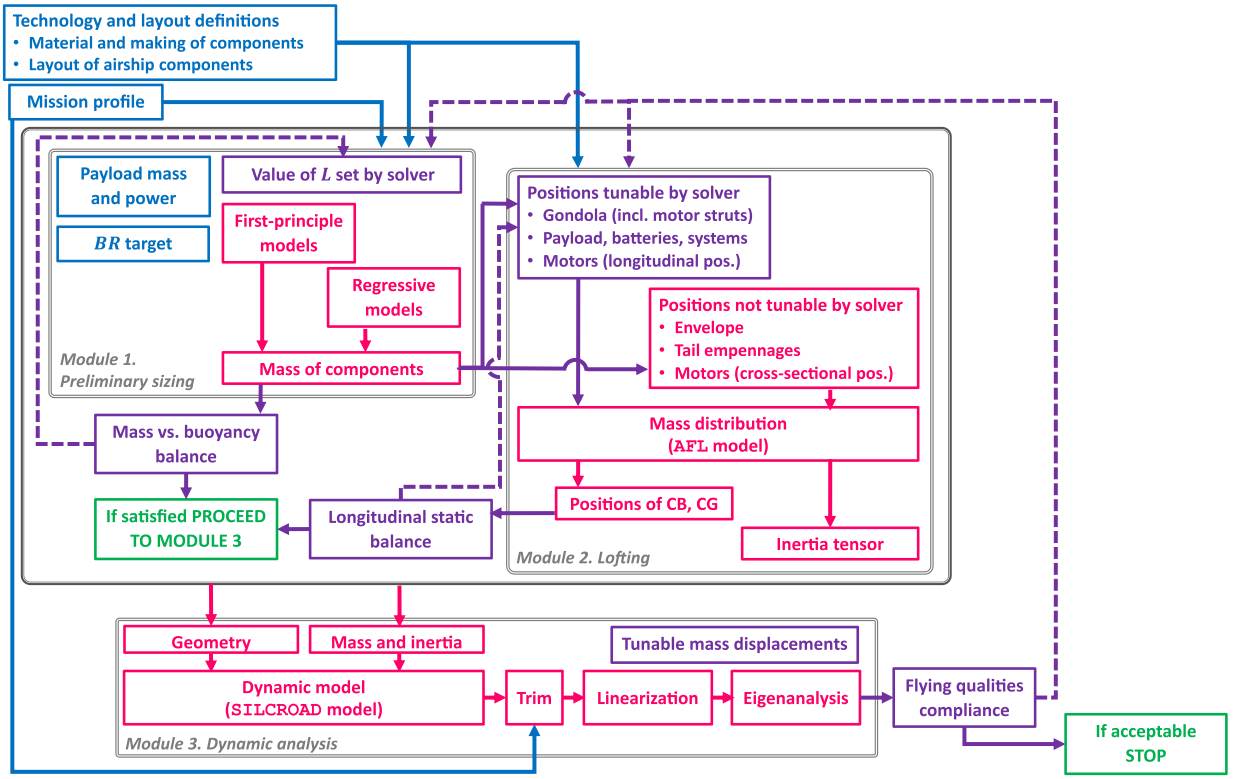

Fig. 4 Conceptual workflow of the unified design methodology.

algorithm, which remains based on the two unknowns L and $\bar{x}$. Clearly, this link increases the computational burden associated with the sizing algorithm, since at every iteration the solver assembles the exact geometrical and inertial model of the candidate airship, corresponding to the current values of the two unknown variables L and $\bar{x}$. However, the output of the synergistic use of the two modules for preliminary sizing and lofting is a design solution capable of capturing the mission goals in terms of power balance and weight-versus-buoyancy balance, featuring a finalized geometrical and inertial sizing accounting for the designer's choices in the layout of all its components such that it accurately satisfies static balance.

The second aspect of major relevance in the scheme proposed above is that of the link between the first two modules and the third one, allowing for the computation of dynamic performance. In practice, the setup of the dynamic model according to the adopted mid-fidelity approach requires additional inputs only related to the aerodynamic and propulsive modeling of the system. Conversely, the information on the mutual positioning of the centers CG and CB and the knowledge of the mass, external volume, and inertial characteristics of the airship are lumped in the static moment and inertia tensors, defined by components by the lofting code, hence readily available. Furthermore, concerning aerodynamic modeling, it was decided to attempt to automate the scaling of the aerodynamic properties with respect to the features of the design. The model considers separately the envelope and the tails, with interference effects modulated by interference factors [11]. The latter are functions of area characteristics of the tail and envelope (actually, the values presented in the literature are obtained from experimental regressions with a validity assured only for some geometries, yet they are assumed here to be valid, also on account of the little effect of changes on the results bound to these quantities). Munk's coefficients for apparent mass and inertia are assumed from tabulated functions of the fineness ratio [31], which is known. The parasite drag of the envelope is a function of the Reynolds number at the top radius of the envelope [33], whereas the crossflow drag coefficient of the envelope and empennages is a function of the Reynolds number and aspect ratio of the fins [34]. Finally, the aerodynamic coefficients of the empennages are obtained from basic lifting surface theory, as functions of the taper and aspect ratios of these components [36]. Therefore, all aerodynamic coefficients can be obtained as functions of quantities in the geometry of the airship, hence defined in the lofting phase.

Propulsion characteristic curves are implemented in this research as functions of the throttle only, employing datasheets of existing motors [37] for creating a shape function of thrust versus throttle setting and scaling it by the nominal value of thrust obtained from the sizing (first two modules), divided by the assigned number of motors N_m.

With the linking of the third module for airship dynamics to the previous two, it is possible to obtain the dynamic performance for each candidate sizing. By assigning a nominal speed for the design (e.g., for the cruise phase), it is possible to solve for static trim in that condition and assemble a linearized model for airship dynamics. From the state matrix, it is possible to extract six characteristic eigenmodes, which for an airship in horizontal symmetric flight feature markedly decoupled longitudinal (namely, pendulum, heave, and surge) and lateral-directional modes (lateral pendulum, side-slip subsidence, and yaw subsidence).

B. Flying Qualities as a Target for Design

With the availability of the eigenvalues of the system, it is possible to attempt to steer the design of the airship toward a desired performance in terms of flying qualities (Fig. 4). In this context, the effort has been focused primarily on two of the six characteristic dynamic modes of the airship that exert the greatest influence on its stability and flight dynamics, namely, the longitudinal pendulum and the side-slip subsidence modes. The relevance of these modes within the overall dynamics of the airship, observed in practice, is supported both by the analytical considerations presented in [15] and by the discussion on the topic provided in [38].

A comprehensive search was carried out for research papers and certification documents that specify the applicable limits and constraints for the two selected characteristic modes to define them as target objectives for the design process. The topic is treated very sporadically, and in a far less accurate way than it is for winged aircraft and rotorcraft. In particular, the CS-30Ts [39] and CS-30Ns

[40] regulations issued by EASA, respectively, for transport- and normal-category airships, as well as the Special Condition SC-GAS [41], only provide qualitative guidelines and general recommendations aimed at mitigating the effects of certain dynamic modes on the overall motion of the airship. They do not, however, establish quantitative thresholds that can be directly employed for design purposes. To overcome this shortcoming, the limits defined in the military aviation standards, namely, MIL-F-8785C [42] and MIL-STD-1797 [43], have been adapted and transposed in this research to the airship domain.

This adaptation was made possible by establishing a functional correspondence between the dynamic modes of airships and those of fixed-wing aircraft. Specifically, a direct analogy can be drawn between the phugoid and the longitudinal pendulum and also between the spiral and the side-slip subsidence modes. The correspondence between the side-slip subsidence and spiral modes lies in their aperiodic lateral-directional nature, both governed by the divergence or recovery of the side-slip motion. In both cases, the dynamics are represented by a real eigenvalue and evaluated through the associated doubling or halving time. Similarly, the longitudinal pendulum and the phugoid are long-period longitudinal modes featuring slow exchanges between potential and kinetic energy and are described by equivalent damping-ratio and natural-frequency indicators. Based on this equivalence, the threshold values of the damping ratio ζ and doubling time T_2 prescribed by the military specifications for winged aircraft were adopted as the numerical objectives of this analysis. In particular, for the spiral mode (associated with the side-slip subsidence), the requirement is a doubling time $T_2 > 20$ s if unstable, whereas for the phugoid (associated with the longitudinal pendulum), $\zeta > 0.04$, or $T_2 > 55$ s if unstable. Despite the similarity in the physical genesis of the two selected modes for the aircraft and airship cases, on account of obvious differences between these platforms, the MIL limits are combined in the procedure envisaged here with reference values of these quantities taken from the measured dynamic behavior of an airship of a general size and mission similar to the one of interest. This is clearly a provisional measure to tackle the potential inconsistency between the performance prescriptions coming from the aircraft domain and the dynamic performance of an airship. Consequently, the adopted target value for each mode was defined as the minimum of the MIL threshold and the corresponding parameter of a reference airship for the class.

The final major component in the setup of a design procedure is the definition of a set of free variables with an effect on the performance of interest, among those potentially tunable in the geometrical and inertial layout of the airship. The two modes under investigation are particularly sensitive to geometric parameters such as the inertia component J_{zz} around the body's vertical axis (along $\boldsymbol{b}_3$), and the vertical distance between the centers of gravity and buoyancy, $h = z_{CG} - z_{CB}$, along the same axis along $\boldsymbol{b}_3$ [15]. In particular, h has a direct effect on the damping of the longitudinal pendulum oscillatory mode, whereas J_{zz} influences the time constant of side-slip subsidence. In order to exert an influence on these quantities, which are not directly tunable, a set of three free parameters has been employed. The first represents the vertical displacement of the gondola from the center of buoyancy, Δz. To explain the other two, consider, as in Fig. 5, splitting each of the masses on board the gondola (i.e., payload, battery, and pressure system) into four equal components and displacing these four parts in a longitudinal and sideward direction. This process preserves the contribution to the center of gravity of the original mass yet alters the inertia in the horizontal plane. The intensities of the displacements, namely, Δx and Δy, are the two final components within the array of tunable parameters.

In this research, an optimal approach has been employed for easier numerical convergence to a design solution, where a composite cost function is defined to simultaneously target longitudinal and lateral-directional flying-quality goals. The following components are correspondingly defined. Considering $(\cdot)^*$ as a target value for a given quantity, for the oscillatory pendulum mode, given the real part σ_{pen} of the eigenvalue, the damping ζ_{pen} and the doubling time $T_{2,pen}$, we have

$$r_{pen}(x;s) = \begin{cases} \mathrm{pos}_k\left(\dfrac{\zeta^* - \zeta_{pen}}{\zeta^*}\right), & \text{if } \sigma_{pen} < 0, \\ \mathrm{pos}_k\left(\dfrac{T^*_{2,pen} - T_{2,pen}}{T^*_{2,pen}}\right), & \text{if } \sigma_{pen} > 0 \end{cases} \tag{6}$$

where $\mathrm{pos}_k(a) = (1/k)\,\ell_n\,(1 + e^{ka})$ is a smooth hinge operator behaving as a differentiable approximation of $\max(0, a)$. Similarly, for the nonoscillatory side-slip subsidence mode represented by the (real) eigenvalue λ_{sss}, assuming $T_{2,sss}$ as its doubling time, we have

$$r_{sss} = \begin{cases} \mathrm{pos}_k\left(\dfrac{T^*_{2,sss} - T_{2,sss}}{T^*_{2,sss}}\right), & \text{if } \lambda_{sss} > 0, \\ 0, & \text{if } \lambda_{sss} < 0 \end{cases} \tag{7}$$

The values of the target quantities ζ^*, $T^*_{2,pen}$, and $T^*_{2,sss}$ are set as the minimum of the values specified by regulations and those of a reference airship, as mentioned, to mitigate the inaccuracy of the adopted regulatory framework, which was not developed for airships and is employed here tentatively.

In addition to the components defined in Eqs. (6) and (7), in order to help keep the design solution in proximity to the baseline obtained from the first two modules before any requirement for flying qualities is applied, a regularization component is added to the functional for optimization, namely,

$$r_{reg} = \frac{\mathrm{Vol}}{\mathrm{Vol}^{(0)}} \tag{8}$$

where the $(\cdot)^{(0)}$ terms refer to the initial design solution, found by launching the first two modules as explained in Sec. II.B.

The functional J_s to be minimized is then

$$J_s = w_{pen}\, r^2_{pen} + w_{sss}\, r^2_{sss} + w_{reg}\, r^2_{reg} \tag{9}$$

where the weights w_{pen}, w_{sss}, and w_{reg} may be set so that the first two are equal and the latter, relative to the regularization component,

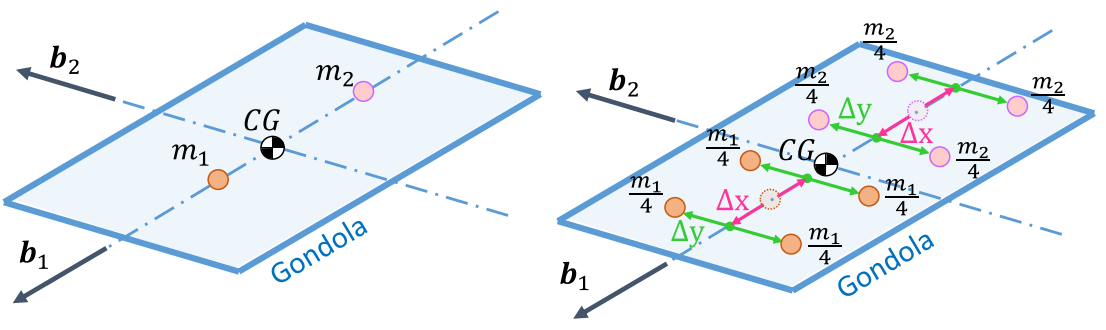

Fig. 5 Explaining the definition of tunable parameters Δx and Δy.

is lower. After defining an array of unknowns $\boldsymbol{x} = \{\Delta z, \Delta x, \Delta y\}$, the solution to the optimization problem is sought formally as

$$\boldsymbol{x}^{\star} = \arg\min_{\boldsymbol{x}} J_s(\boldsymbol{x}) \tag{10}$$

The optimization parameters are bounded so that the positions of the masses on the gondola do not exceed the geometrical boundaries (length and width) of the latter, whereas the vertical placement of the gondola does not conflict with the envelope.

As shown in Fig. 4, the numerical solution of the design problem considering the unified design procedure therefore features two nested iterative procedures and is a function of five scalar unknowns. The internal iteration is a function of the envelope length L and the displacement $\bar{x}$, which are determined by running the first two modules, such that they satisfy weight balance and static balance, within a solver for a non-linear system of two scalar equations. The solution at this phase does not account for flying qualities. Then the external iterative procedure, by acting on the components of $\boldsymbol{x}$, is employed to steer the positioning of the masses on board. At the end of an external iteration, the value of J_s is determined, and the values of the array of displacements $\boldsymbol{x}$ updated toward reaching the minimum of the functional before launching a new iteration. The overall unified procedure, based on a regular functional, does not pose significant convergence issues when employing a standard gradient-based numerical algorithm for the optimization.

IV. Case Study

The case presented in this research is based on the small-scale preliminary study airship built within project IPROP for experimenting with different topologies of the motors and tail [9]. This is shown in Fig. 6, respectively, as represented in a commercial CAD software package and in a photograph (tails are not present in these representations). The main driver behind project IPROP is the inclusion of atmospheric ionic thrusters on an airship. This type of propulsion, the focus of a massive characterization effort within the project [44,45], promises to deliver moderate thrust starting from a voltage difference in a matrix of suitably distributed wires with no moving parts. Such a magnitude of thrust, while not sufficient for propelling winged aircraft, on the other hand, shall allow one to propel and steer an airship in flight. Furthermore, the lack of moving parts in the power supply (i.e., battery) and thrust-generation systems allows one to greatly reduce complexity and noise, thus, respectively, boosting TBO and reducing detectability. Correspondingly, this type of technology is intended as an enabler for high-altitude unmanned airships and is especially valuable for military applications [24]. In order to eliminate any moving parts on board, both for the sake of constructive simplicity (positively impacting TBO) and for reducing residual noise from actuators, within IPROP an accent has been placed on the thrust-controlled flight paradigm. The outcome of preliminary studies on a thrust-controlled airship layout has shown that this is indeed feasible [5–7], yet their results remain limited in scope by the lack of practical testing. To fill this gap, the small-scale preliminary demonstrator was designed from the start to allow the reproduction of several potential arrangements of the thrusters and of the tail, so as to steer the choice of the layout of a full-scale prototype, which will be manufactured as a technological demonstrator for atmospheric ionic thrusters for low-altitude flight as a final milestone of project IPROP. To reduce the cost and miniaturize the small-scale prototype with respect to the full-scale demonstrator, it was elected to put on board simple electromechanical groups (instead of ionic thrusters), which nonetheless allow one to capture the effect of the overall layout of the thrusters on trim and controlled dynamics.

For this purpose, the gondola has been designed with four curved arms, running upward along the cross section of the envelope. Both of these components are assembled from modules of balsa wood (nominal density of 140 $\mathrm{kg/m^3}$), with a cross section of 3.0×3.0 cm for the gondola perimeter frame and curved arms, and 3.0×1.0 cm for the internal frames of the gondola. The gondola can be shifted back and forth by attaching it to four anchor points, chosen from a set of eight per side, prepared in advance symmetrically on the two sides of the airship (see Figs. 6 and 7). A similar approach has been followed for the tails, where an abundant number of patches has been prepared, allowing the designer to experiment with different numbers and positions of the empennages. The construction of the latter is based on polystyrene panels (density 22 $\mathrm{kg/m^3}$), whereas experiments with more elaborate balsa frames with an Oralight cover, forming an aeronautical beam with a better aerodynamic shape, are currently underway. The gondola and empennages are attached to the envelope via polypropylene cables (nominal density 920 $\mathrm{kg/m^3}$). The gondola and the arms offer some tens of predefined anchor points for the motors, as can be seen in Fig. 7. Six electric motors (T-Motor MN4004-19 KV400 with independent ESCs [37]) and propellers have been employed, giving a nominal thrust of 1.01 N each at 100% throttle. Notably, as stated, the tail empennages do not have any deflectable trailing-edge surfaces, thus requiring the use of differential thrust to trim, propel, and steer the airship [6,7].

The envelope is made of polyurethane (density 1120 $\mathrm{kg/m^3}$ and thickness 0.18 mm), with 12 longitudinal segments and no diaphragms, arranged according to an axis-symmetric shape defined by a seventh-order polynomial drawn in the longitudinal plane. The airship is filled with helium as a lifting gas, and there is no pressure-management system on board. Interestingly, the choice of the envelope material, offering a rather penalizing weight-to-area performance, has been driven by the need to accelerate production and ensure minimal helium leakage for cost-efficient operation of this preliminary prototype. The relatively thick envelope material is easy to solder and to attach patches to while effectively containing lifting gas leakage. On the downside, the combination of the relatively high mass density of the envelope material and the need to reduce the overall length of the airship to allow indoor (i.e., all-weather,

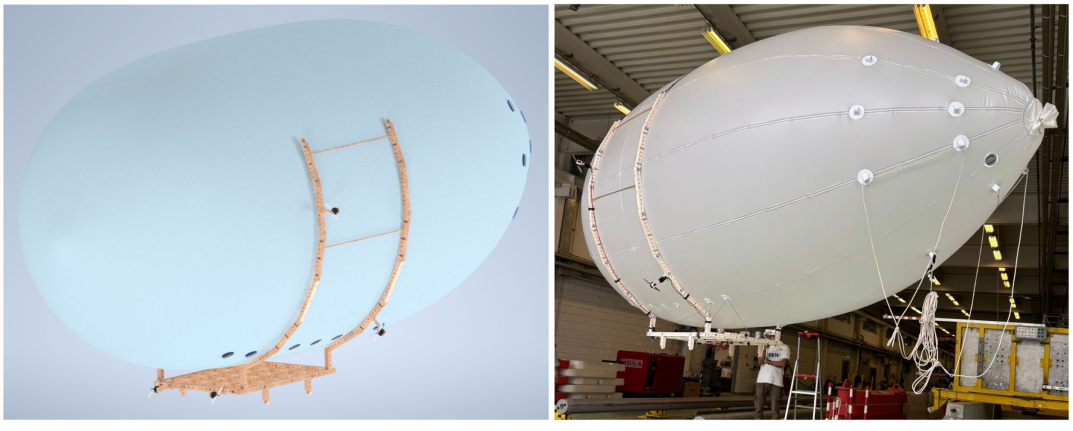

Fig. 6 Study airship developed within project IPROP [9]. Left: commercial CAD representation. Right: photograph during assembly operations.

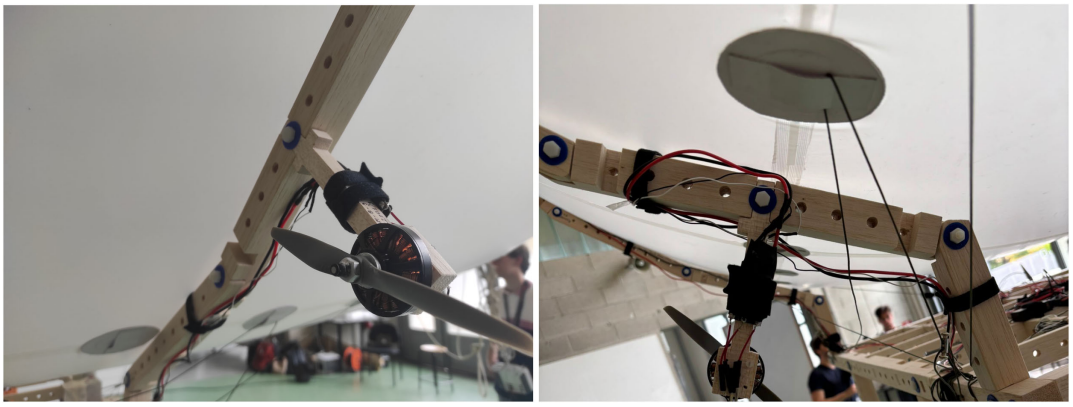

Fig. 7 Detail view of the propeller and of the gondola patches. Left: motor, propeller, and attachment points on the frame. Right: gondola patch with attachment cable.

year-round) operations has forced the designers to attain a corresponding increase in envelope volume (such that it compensates for the weight of the airship) mainly by means of an increase in envelope radius. This, in turn, has produced a rather low fineness ratio, which clearly penalizes the quality of the dynamic response of the airship (which intuitively shall tend to behave more like a buoyant sphere than a longitudinally-developed solid).

Knowledge of the materials and properties of the components has allowed the employment of accurate first-principle models for mass predictions within the preliminary sizing phase. The actual preliminary sizing of the airship has been carried out employing `Morning Star` in its basic implementation, i.e., with only the length of the envelope L as an unknown (Sec. II.A.1). The target buoyancy ratio BR for the design was set to 1.0, leaving much room for experimentation with different values of this parameter, simply adding dead weight to the suitably designed large gondola. For the baseline sizing, the empennages considered are four, in a standard cruciform layout (among the many enabled by the abundant anchor points). The airship is conceived for indoor testing, as stated, and the design mission features a range of 500 m at a nominal speed of 3 m/s and at an altitude of 5 m above ground (at the elevation of the testing site in Milan, Italy). Climb and descent (actually very short and of little relevance in this design) are flown at the same speed as the cruise.

A. Preliminary Sizing and Detailed Static Balance

For the actual construction of this airship, static balance has been relegated to the practical tuning phase, with the weight of the batteries and payload (onboard computer) positioned by hand to keep the airship in static equilibrium for a specific positioning of the gondola, tail empennages, and motors. In the context of this research, instead, the two modules composing the inner loop are employed for a first functional test of the proposed design procedure to yield a statically balanced lofting of the airship. A baseline layout has been selected, where the empennages are fixed and have no incidence. Two motors are aligned in the plane of symmetry, attached to the bottom of the gondola, with an up-tilt 10 deg for easing longitudinal trimming. The other four motors are located, two on the front arms and two on the back arms, all above the longitudinal axis of the envelope, at different vertical positions for the front and back pairs, respectively. Considering as a reference condition the cruise phase in the mission profile (velocity of 3 m/s and altitude of 5 m), and a target buoyancy ratio BR $= 0.995$, the first two modules in the unified sizing procedure are employed (Fig. 4), solving for both parameters L and $\bar{x}$. The sized output, as represented within `AFL`, is shown in Fig. 8. The values of the length L and position $\bar{x}$ solving a design based on the first two modules, as well as other basic design outputs, are shown in Table 1.

An accurate measure of the accuracy of the position $\bar{x}$ for positioning the movable masses on the gondola tray was not possible on the actual machine, yet, as a matter of fact, the batteries and payload (onboard computer) were positioned at the front of the gondola, less

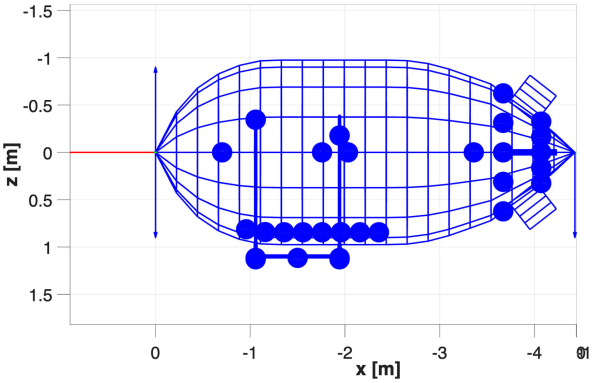

Fig. 8 Representation of the design of the IPROP study airship resulting from the first two modules of the design procedure (Fig. 4) within `AFL`. Dots: lumped masses. Lines: finite bodies.

Table 1 Results of preliminary sizing and static balance, employing the first two modules of the unified sizing procedure for the IPROP study airship

Quantity	Real airship	Predicted value	Percent difference, %
Envelope length, L, m	4.496	4.424	−1.60
Tunable mass shift, $\bar{x}$, m	—	0.0437	—
Airship take-off mass, M_{TO}, kg	11.36	10.99	−3.3
Airship volume, Vol, m^3	9.12	8.84	−3.1

than 8 cm from the estimated position of the center of gravity, obtained via empirical testing. The differences between predicted and actual values are the result of both a different design procedure in the construction of the real prototype and the actual inaccuracy of the prediction method. With this notion, it can be speculated that, in this particular case, the simultaneous solution of L and $\bar{x}$, instead of only the envelope length L as performed for the actual machine, does not largely impact the global sizing.

B. Assessing the Dynamic Performance of the Prototype

Before launching the unified design procedure, encompassing the iterative use of the third module for dynamic computation, the latter was employed for an estimation of the flying qualities of the baseline design solution just obtained. A topological representation of the `SILCROAD` model employed for the task is presented in Fig. 9. Notably, the tail empennages are represented only through their surface area and positioning (the visualization does not account for their actual shape). As anticipated, the reference values of an airship of comparable size have been considered as candidates for comparison,

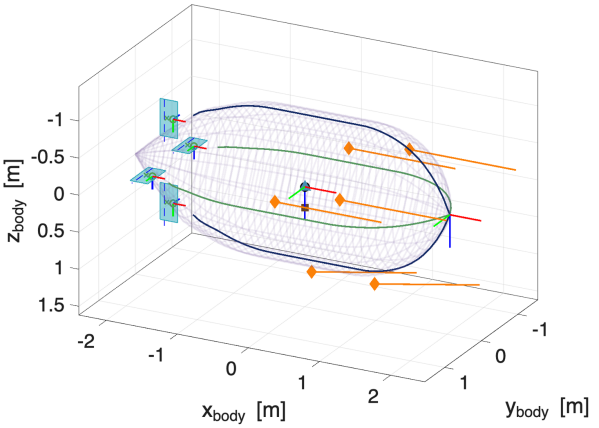

Fig. 9 Representation of the IPROP study airship for dynamic analysis within SILCROAD. Amber vectors represent thrust.

Table 2 Results of dynamic analysis employing the third module of the unified procedure (a model of the airship in SILCROAD environment) for the IPROP study airship

Quantity	Value	Target
Pendulum damping, ζ_{pen}	0.078	0.040
Side-slip doubling time, $T_{2,\text{sss}}$, s	1.161	20
Pendulum component of cost function, r_{pen}	$O(10^{-5})$	0
Side-slip component of cost function, r_{sss}	0.942	0

in lieu of those from MIL regulations. Those pertaining to the *Lotte* airship, for which the eigenvalues are available as functions of the airspeed [15], have been considered in particular. However, for the case at hand (3 m/s), the requirement from the regulations is, in turn, more stringent.

The results of this test are reported in Table 2, highlighting a dynamic performance that is especially critical in terms of side-slip subsidence (often unstable on airships), where the doubling time is significantly above the target value from the regulations. Conversely, the value of the damping of the (stable) longitudinal pendulum is higher than required.

C. Sizing Solution According to the Unified Procedure

It is then interesting to check the outcome of the proposed unified design procedure, taking dynamic performance into account. The full design algorithm has been employed (Fig. 4), in particular considering for the optimization a gradient-based method with a multi-start option based on eight randomly selected initial conditions. The values of the weights in Eq. (9) have been set to $w_{\text{pen}} = w_{\text{sss}} = 1.0$ and $w_{\text{reg}} = 10^{-3}$, respectively. The variability of the optimal J_s depending on the initial condition is always below $O(10^{-6})$, suggesting a generally good regularity of the cost function. It is interesting to study a typical convergence history of the optimizer, presented in Fig. 10 as obtained for one of the initial conditions, and leading to the final design solution (as stated, the optimum is captured with good accuracy irrespective of the initial condition). The latter is presented in Table 3.

Considering Fig. 10, the cost function J rapidly decreases during the early steps, before reaching a steady convergence plateau once this equilibrium is achieved.

Both the geometrical parameter h and the inertial parameter J_{zz} initially decrease as the optimizer seeks to minimize the pitch-related pendulum effect and refine the coupling between the centers of buoyancy and mass. This initial trend reflects the stabilizing action of the optimizer in improving the arrangement of the masses while maintaining static balance. However, in the final iterations, a modest yet distinct increase in J_{zz} can be observed. This final rise is the result of a redistribution of the internal subsystems toward the outermost admissible boundaries of the gondola volume to enhance

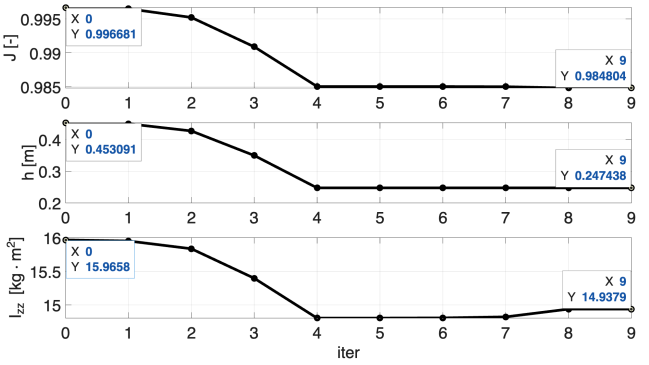

Fig. 10 History of convergence over an optimally solved unified design procedure.

Table 3 Results of the unified design algorithm for the IPROP study airship

Quantity	Baseline value	Optimal value
Displacement of gondola along $\boldsymbol{b}_3$, Δz, m	1.100	0.975
Displacement of on-gondola masses along $\boldsymbol{b}_1$, Δx, m	0.000	0.442
Displacement of on-gondola masses along $\boldsymbol{b}_2$, Δy, m	0.000	0.341
Airship inertia along $\boldsymbol{b}_3$, J_{zz}, kg · m^2	14.77	14.94
Vertical offset of CG vs CB, h, m	0.280	0.247
Envelope length, L, m	4.424	4.410
Airship take-off mass, M_{TO}, kg	10.99	10.89
Airship volume, Vol, m^3	8.84	8.75
Pendulum damping, ζ_{pen}	0.078	0.045
Side-slip doubling time, $T_{2,\text{sss}}$, s	1.161	1.167

yaw inertia and thereby improve the damping characteristics associated with the spiral mode. The increase in J_{zz}, although moderate, plays a crucial role in mitigating the tendency of the airship toward spiral divergence, particularly in configurations where the tail surfaces provide limited aerodynamic stabilization.

The small variations observed in the overall envelope length L and total mass M_{TO} are instead attributable to the secondary optimization objective of regularization, which slightly adjusts the global sizing while preserving the geometric proportions and global consistency of the baseline solution. These changes confirm that the optimizer operates cohesively within the constraints of the sizing routine, maintaining the physical plausibility of the solution. The resulting optimized baseline thus represents a dynamically enhanced and physically consistent solution to static equilibrium, within the limits of the prototype geometry.

D. Parameterized Study for Different Mission Settings

The figures presented in this section collectively illustrate the results of the parametric optimization study conducted on the baseline configuration, highlighting how the reference flight velocity V and buoyancy ratio BR affect the physical characteristics, dynamic response, and compliance with the selected certification standards of the airship. The discussion follows a logical sequence, beginning with the overall certification performance, then examining the variations in the main dynamic parameters, and concluding with the geometric and modal implications that arise across the operational field.

The certification map in Fig. 11 provides an immediate overview of the compliance landscape. It reveals that the admissible region in which the optimized configurations satisfy the MIL-derived stability requirements is notably narrow. The green area, corresponding to full compliance, is virtually absent, while most of the operational domain falls within the yellow (intermediate) or red (fail) regions. This distribution indicates that, as the flight velocity increases beyond approximately 4 m/s and the buoyancy ratio approaches

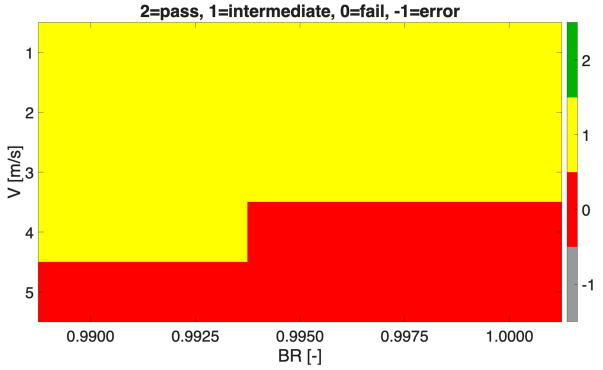

Fig. 11 Pass vs. fail map of airship design solutions for changing buoyancy ratio BR and reference speed V.

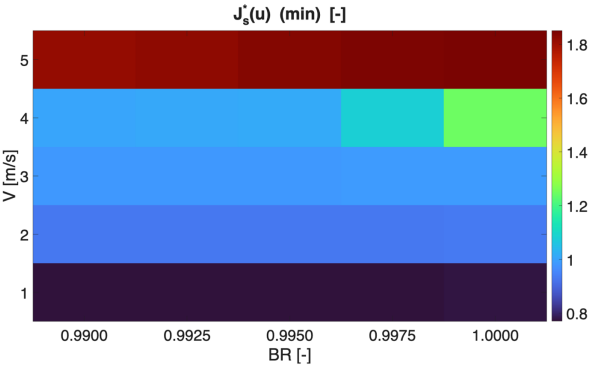

Fig. 13 Optimal value of cost function $J_s^\star$ for changing buoyancy ratio BR and reference speed V.

unity, the vehicle progressively departs from the certified stability margins. The underlying reason lies in the combined effect of greater aerodynamic loads and varying buoyant force, which constrains the attainable stability characteristics. Thus, the map highlights that only at low V and low BR can the configuration operate close to acceptable certification limits, effectively defining the feasible and semicompliant flight regions.

Following this global assessment, the heat maps in Fig. 12 of the percentage variations of parameters h and J_{zz} relative to the baseline provide deeper insight into how the optimizer compensates for these changing reference conditions. The map of Δh^{opt} displays a strong, monotonic increase in h with velocity, reaching variations exceeding 100% at higher velocities V. This growth is physically consistent: as aerodynamic forces intensify, a greater vertical separation between the centers of mass and buoyancy is required to restore longitudinal stability. Conversely, under near-static, low-speed conditions, such separation is reduced, as the buoyant equilibrium itself ensures sufficient static balance. A parallel but more moderate trend can be observed in the map of $\Delta J_{zz}^{\text{opt}}$, where the yaw inertia increases by approximately 5–9% with rising V and BR. This reflects the internal mass redistribution strategy of the optimizer, which enhances lateral-directional stability and damping as the dynamic regime becomes more demanding. The steeper gradient along the velocity axis in both plots confirms that speed is the dominant parameter influencing both inertia and equilibrium, overshadowing the smaller effects of buoyancy ratio variations. These results validate the expected physical response of semi-buoyant vehicles, for which increasing dynamic pressure necessitates a proportional rise in stabilizing lever arms and inertial resistance. In addition, the increase in operational speed represents the primary parameter influencing the sizing of the airship itself.

The behavior of the cost function J_s mirrors these observations. The corresponding map in Fig. 13 shows that the minimum values of J_s are achieved for low-speed, slightly underbuoyant conditions, whereas higher velocity V and buoyancy ratio BR lead to a steady increase. This growth in J_s signifies a progressive departure from the ideal stability targets. Within the defined operational field, slow flight with a buoyancy ratio slightly below unity yields the most advantageous trade-off between the components of the considered cost function.

Finally, the analysis of the modal parameters $T_{2,\text{sss}}$ and ζ_{pen} in Fig. 14 provides a direct interpretation of the dynamic stability of the airship. The map of the side-slip subsidence mode time constant $T_{2,\text{sss}}$ reveals a steady decrease with increasing velocity V, denoting a faster and less stable lateral response at higher speeds. In contrast, the longitudinal pendulum damping ratio ζ_{pen} exhibits a marked decline at elevated V and BR, indicating the emergence of lightly damped longitudinal oscillations typical of near-neutral or marginally unstable regimes. The correspondence between these two quantities confirms the physical realism of the numerical model: as is typical of airships [15], aerodynamic forces grow in magnitude, and both pitch and yaw modes approach the threshold of dynamic instability.

It is also worth noting that the side-fslip subsidence mode constraint is never satisfied across the entire operational domain analyzed. This outcome can be attributed primarily to the particular geometry of the demonstrator under investigation, characterized by a rather bulky and compact hull shape, relatively undersized tail surfaces, and reliance on differential thrust only to guarantee trim (as mentioned, there is no provision for deflectable surfaces on the empennages). The persistent violation of the spiral stability criterion directly affects the interpretation of the results, as it causes the certification map (Fig. 11) and the damping ratio plot of the longitudinal pendulum mode (Fig. 14) to become nearly coincident. From these visualizations, it is evident that at the highest investigated speed, $V = 5$ m/s, the longitudinal pendulum mode turns unstable and fails to meet even the fundamental certification requirement of $T_{2,\text{pen}} > 55$ s. Similarly, for higher buoyancy ratios at $V = 4$ m/s, the heat map clearly shows

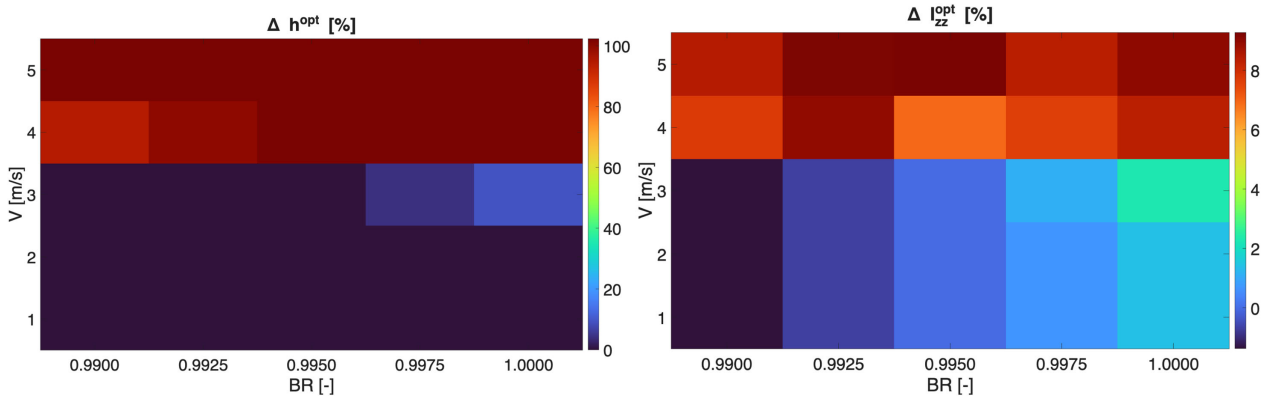

Fig. 12 Change in h^{opt} (left) and J_{zz}^{opt} (right) in the optimal design solution with respect to a baseline nonoptimized solution, for changing values of buoyancy ratio BR and reference speed V.

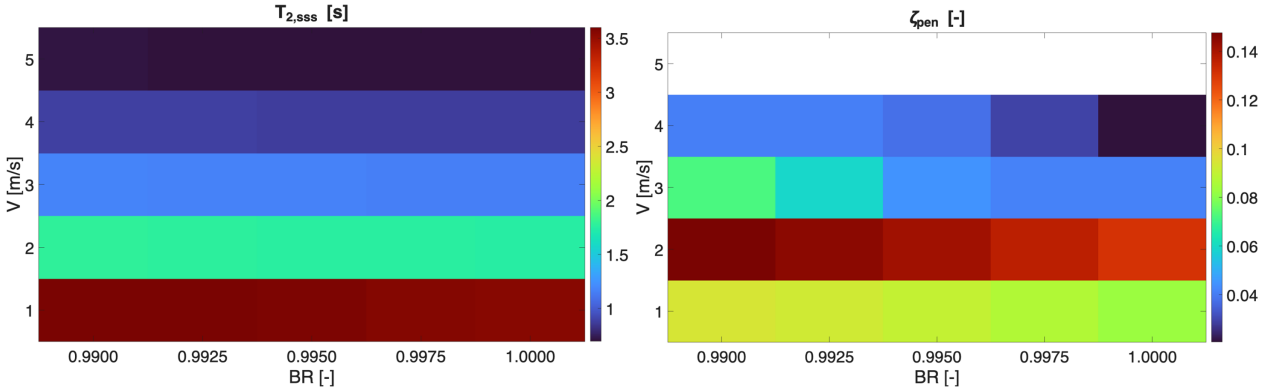

Fig. 14 Optimal values of optimal modal parameters $T_{2,sss}$ and ζ_{pen} for changing buoyancy ratio BR and reference speed V.

that the pendulum damping ratio ζ_{pen} falls below the minimum target value of 0.04, confirming the same degradation of dynamic behavior observed in the overall compliance map.

Together, the information just presented outlines a coherent and physically sound narrative. As the airship transitions from low-velocity-V, low-buoyancy-ratio-BR conditions to faster or more neutrally buoyant regimes, its dynamic stability progressively degrades. Moreover, it is particularly significant that the largest variations observed in h^{opt} and J_{zz}^{opt} occur precisely in the same region where the pendulum mode begins to destabilize, that is, at the highest investigated velocities. This correlation suggests that the optimizer attempts to compensate for the growing instability of the longitudinal mode through geometric and inertial adjustments, though the inherent aerodynamic inefficiencies of the demonstrator ultimately prevent full recovery of the stability margins. This interplay between the aerodynamic, inertial, and geometric responses confirms the robustness of the implemented optimization framework and its capability to autonomously reproduce the complex couplings that govern semi-buoyant flight dynamics. The presented results thus represent a validation of both the proposed design methodology and its physical fidelity across the entire operational envelope considered.

V. Conclusions

The airship design methodology introduced in the present paper aims to account for diverse design objectives simultaneously within a unified automatic sizing procedure. Baseline methods, already documented in the literature, allow the designer to work out a preliminary sizing solution such that it satisfies a buoyancy-capacity target while implicitly granting mission constraints, power balance, and structural integrity. By additionally linking tools, respectively, for lofting/detailed inertial modeling and for dynamic simulation, this research proposes a comprehensive environment in which the further information required from the designer (essentially, the geometry and mass properties of components in the airship layout) enables an automatic search for a design solution in which static balance as well as a level of flying qualities are directly accounted for.

For the setup of an automated procedure, a modular method has been envisaged. Concerning flying qualities, within the still preliminary framework of requirements available from regulations (in particular for small-scale unmanned machines, which are mostly of interest in the current market scenario), an optimal approach is employed so as to obtain a design solution that comes as close as possible to the requirements yet produces a result even in cases in which an exact match with respect to a desired flying quality level is unreachable.

A case study inspired by the data available from an existing unmanned airship prototype has been presented. The application of a design routine taking into account longitudinal balance to the mission requirements and technological features of that prototype provides data that do not depart from those of the real machine. This shows that the design procedure aligns with reality and that the additional requirement of static balance, not accounted for at a design level when the real machine was designed, does not bring about dramatic modifications. Conversely, the application of the complete procedure, including requirements on flying qualities accounted for in an optimal way (i.e., not exactly), produces results that, although consistent with the previous solution, show that the topology of the prototype is unlikely to meet an acceptable level of dynamic performance. This is generally true also when two relevant design parameters, namely, nominal velocity and buoyancy ratio, are perturbed in a parameterized fashion. This was expected, since the machine at hand has been experimentally tested and found to be rather unsatisfactory in terms of maneuverability, which was not a major driver in its design.

The procedure proposed herein has been tested on alternative candidate topologies, not shown for brevity (purely hypothetical, not based on a real prototype), displaying again consistent results and, for an increased fineness ratio of the envelope, better chances of meeting flying quality requirements under the same constraints considered in this work.

An additional work package developing the present work will be dedicated to the addition of solar cells as well as ballonets, enabling the design of a machine reaching the higher layers of the atmosphere, with the same level of detail shown in this research while accounting for such additional components, which are very relevant for stratospheric lighter-than-air flight.

Data Availability

The dataset corresponding to the graphical results presented in this research is publicly available on Zenodo with 10.5281/zenodo.19366310.

Acknowledgments

This project has received funding from the European Union's Horizon Europe Research and Innovation Programme under Grant Agreement No. 101098900. Views and opinions expressed are, however, those of the authors only and do not necessarily reflect those of the European Union or the European Innovation Council and SMEs Executive Agency (EISMEA). Neither the European Union nor the granting authority can be held responsible for them. The contributions of Andrea Gaiani and Luca Spinelli, who were responsible for the design and manufacture of the airship prototype employed in the case study, are gratefully acknowledged.

References

[1] Riboldi, C. E. D., and Fanchini, L., "Assessing the Technical–Economic Feasibility of Low-Altitude Unmanned Airships: Methodology and Comparative Case Studies," *Aerospace*, Vol. 12, No. 3, 2025, p. 244. https://doi.org/10.3390/aerospace12030244

[2] Riboldi, C. E. D., and Gualdoni, F., "An Integrated Approach to the Preliminary Weight Sizing of Small Electric Aircraft," *Aerospace Science and Technology*, Vol. 58, 2016, pp. 134–149. https://doi.org/10.1016/j.ast.2016.07.014

[3] Riboldi, C. E. D., "An Optimal Approach to the Preliminary Design of Small Hybrid-Electric Aircraft," *Aerospace Science and Technology*,

Vol. 81, 2018, pp. 14–31.
https://doi.org/10.1016/j.ast.2018.07.042
[4] Riboldi, C. E. D., "Energy-Optimal Off-Design Power Management of Hybrid-Electric Aircraft," *Aerospace Science and Technology*, Vol. 95, 2019, pp. 1–16.
https://doi.org/10.1016/j.ast.2019.105507
[5] Riboldi, C. E. D., and Rolando, A., "Layout Analysis and Optimization of Airships with Thrust-Based Stability Augmentation," *Aerospace*, Vol. 9, No. 7, 2022, p. 393.
https://doi.org/10.3390/aerospace9070393
[6] Riboldi, C. E. D., and Rolando, A., "Thrust-Based Stabilization and Guidance for Airships Without Thrust-Vectoring," *Aerospace*, Vol. 10, No. 4, 2023, p. 344.
https://doi.org/10.3390/aerospace10040344
[7] Riboldi, C. E. D., and Rolando, A., "Autonomous Flight in Near Hover and Hover for Thrust Controlled Unmanned Airships," *Drones*, Vol. 7, No. 9, 2023, p. 545.
https://doi.org/10.3390/drones7090545
[8] Chen, L., Zhang, H., and Duan, D. P., "Control System Design of a Multivectored Thrust Stratospheric Airship," *Proceedings of the Institution of Mechanical Engineers, Part G: Journal of Aerospace Engineering*, Vol. 228, No. 11, 2014, pp. 2045–2054.
https://doi.org/10.1177/0954410013513568
[9] Riboldi, C. E. D., Belan, M., Cacciola, S., Terenzi, R., Trovato, S., Usuelli, D., and Familiari, G., "Preliminary Sizing of a Low-Altitude Airship Including Ion-Plasma Thrusters," *34th Congress of the International Council of the Aeronautical Sciences (ICAS2024)*, Paper 0649, Sept. 2024, pp. 1–20.
[10] Miloh, T., "Forces and Moments in a Tri-Axial Ellipsoid in a Potential Flow," *Israel Journal of Technology*, Vol. 11, 1973, pp. 63–74.
[11] Jones, S. P., and DeLaurier, J. D., "Aerodynamic Estimation Techniques for Aerostats and Airships," *Journal of Aircraft*, Vol. 20, No. 2, 1982, pp. 120–126.
https://doi.org/10.2514/3.44840
[12] Gomes, S. B. V., "An Investigation of the Flight Dynamics of Airships with Application to the YEZ-2A," Ph.D. Thesis, Cranfield Univ., Cranfield, U.K., 1990.
[13] Lutz, T., Funk, P., Jacobi, A., and Wagner, S., "Summary of Aerodynamic Studies on the Lotte Airship," *4th International Airship Conference and Exhibition*, 2002, pp. 1–12, 2002.
[14] Kämpf, B., "Flugmechanik und Flugregelung von Luftschiffen," Ph.D. Thesis, Univ. of Stuttgart, Stuttgart, Germany, 2004.
https://doi.org/10.18419/opus-3715
[15] Kornienko, A., "System Identification Approach for Determining Flight Dynamical Characteristics of an Airship From Flight Data," Ph.D. Thesis, Univ. of Stuttgart, Stuttgart, Germany, 2006.
https://doi.org/10.18419/opus-3731
[16] Carichner, G. E., and Nicolai, L. M., "Fundamentals of Aircraft and Airship Design," AIAA Education Series, AIAA, Reston, VA, 2013.
[17] Smith, S., Fortenberry, M., Lee, M., and Judy, R., "HiSentinel80: Flight of a High Altitude Airship," *11th AIAA Aviation Technology, Integration, and Operations (ATIO) Conference*, AIAA Paper 2011-6973, 2011.
https://doi.org/10.2514/6.2011-6973
[18] Smith, I. S., "HiSentinel & Stratospheric Airship Design Sensitivity," *Keck Institute for Space Studies (KISS) Workshop*, 2013, pp. 1–23.
[19] FloFleet, Via Sebenico 24, 20124 Milan, Italy, https://www.flofleet.com [retrieved Jan. 2026].
[20] Roboloon, Nobelstraße 15, 70569 Stuttgart, Germany, https://www.roboloon.com [retrieved Jan. 2026].
[21] Kelluu Oy, Metallimiehentie 4, 80330 Reijola, Finland, https://kelluu.com [retrieved Jan. 2026].
[22] Sceye Inc., 50 George Applebay Way, Building 200, Moriarty, NM 87035, New Mexico, https://sceye.com [retrieved Jan. 2026].
[23] IPROP Grant ID: HORIZON-EIC-2022-PATHFINDEROPEN-01 - www.iprop-Project.eu, "Ionic Propulsion in the Atmosphere," 2023–2027
[24] Riboldi, C. E. D., Rolando, A., Cacciola, S., Regazzoni, G., and Spadafora, I., "On the Optimal Preliminary Design of High-Altitude Airships: Automated Procedure and the Effect of Constraints," *Aerospace Europe Conference 2023 - 10th EUCASS - 9th CEAS*, 2023, pp. 1–15.
https://doi.org/10.13009/EUCASS2023-024
[25] Riboldi, C. E. D., Rolando, A., and Regazzoni, G., "On the Feasibility of a Launcher-Deployable High-Altitude Airship: Effects of Design Constraints in an Optimal Sizing Framework," *Aerospace*, Vol. 9, No. 4, 2022, pp. 1–37.
https://doi.org/10.3390/aerospace9040210
[26] Riboldi, C. E. D., Belan, M., Cacciola, S., Terenzi, R., Trovato, S., Usuelli, D., and Familiari, G., "Preliminary Sizing of High-Altitude Airships Featuring Atmospheric Ionic Thrusters: An Initial Feasibility Assessment," *Aerospace*, Vol. 11, No. 7, 2024, p. 590.
https://doi.org/10.3390/aerospace11070590
[27] Riboldi, C. E. D., and Marcora, D., "Feasibility and Trade-Offs in the Design of an Airship for Martian Exploration," *Aerospace Science and Technology* (Accepted for publication).
[28] Riboldi, C. E. D., Belan, M., Terenzi, R., and Zhao, Q., "Optimal Topology of a Small-Scale Airship: A Study in Virtual Environment," *11th European Conference for Aeronautics and Astronautics (EUCASS2025)*, 2025, pp. 1–13.
https://doi.org/10.13009/EUCASS2025-461
[29] Drob, D. P., et al., "An Empirical Model of the Earth's Horizontal Wind Fields: HWM07," *Journal of Geophysical Research, Space Physics*, Vol. 113, 2008, Paper A12304, pp. 1–18.
https://doi.org/10.1029/2008JA013541
[30] Drob, D. P., et al., "An Update to the Horizontal Wind Model (HWM): The Quiet Time Thermosphere," *Earth and Space Science*, Vol. 2, No. 7, 2015, pp. 301–319.
https://doi.org/10.1002/2014EA000089
[31] Munk, M. M., "The Aerodynamic Forces on Airship Hulls," NACA TR 184, 1926.
[32] Bateman, H., "The Inertial Coefficients of an Airship in Frictionless Fluid," NACA TR 164, 1924.
[33] Hoerner, S. F., *Fluid-Dynamic Drag*, Hoerner Fluid Dynamics, 1965.
[34] Wardlaw, A., "High Angle of Attack Missile Aerodynamics," Advisory Group for Aerospace Research and Development (AGARD), 1979.
[35] Pamadi, B. N., *Performance, Stability, Dynamics, and Control of Airplanes*, AIAA Education Series, AIAA, Reston, VA, 2004.
[36] Fink, R., "USAF Stability and Control DATCOM," Flight Dynamics Laboratory, Air Force Wright Aeronautical Laboratories, Wright-Patterson AFB, OH, 1978.
[37] T-MOTOR, No. 3399 Ziyang Ave., Nanchang, Jiangxi, P.R. China. 330096, https://store.tmotor.com [retrieved Jan. 2026].
[38] Khoury, G. A., *Airship Technology*, Cambridge Aerospace Series, Cambridge Univ. Press, New York, 2012.
[39] Various, "Certification Specifications for Transport Category Airship - CS-30T," EASA, 2003.
[40] Various, "Certification Specifications for Normal and Commuter Category Airship - CS-30N," EASA, 2003.
[41] Various, "Special Conditions Gas Airships - SC-GAS," EASA, 2022.
[42] Various, "Military Specification: Flying Qualities of Piloted Airplanes - MIL-F-8785C," USAF, 1980.
[43] Various, "Military Specification: Flying Qualities of Piloted Airplanes - MIL–STD-1797," USAF, 1997.
[44] Belan, M., Terenzi, R., Trovato, S., and Usuelli, D., "Effects of the Emitters Density on the Performance of an Atmospheric Ionic Thruster," *Journal of Electrostatics*, Vol. 120, 2022, Paper 103767.
https://doi.org/10.1016/j.elstat.2022.103767
[45] Kahol, O., Belan, M., Pacchiani, M., and Montenero, D., "Scaling Relations for the Geometry of Wire-to-Airfoil Atmospheric Ionic Thrusters," *Journal of Electrostatics*, Vol. 123, 2023, Paper 103815.
https://doi.org/10.1016/j.elstat.2023.103815

B. E. Thompson
Associate Editor